Assessing the readiness of numerical relativity for LISA and 3G detectors

Deborah Ferguson[1,2] Karan Jani[3] Pablo Laguna[1,2] and Deirdre Shoemaker[1,2]

[1]*Center for Relativistic Astrophysics and School of Physics,*
Georgia Institute of Technology, Atlanta, Georgia 30332, USA
[2]*Center for Gravitational Physics and Department of Physics,*
The University of Texas at Austin, Austin, Texas 78712, USA
[3]*Department of Physics and Astronomy, Vanderbilt University, Nashville, Tennessee 37235, USA*

Future detectors such as the Laser Interferometer Space Antenna promise signal-to-noise ratios potentially in the thousands and data containing simultaneous signals. Accurate numerical relativity waveforms will be essential to maximizing the science return. A question of interest to the broad gravitational wave community is: Are the numerical relativity codes ready to face this challenge? Towards answering this question, we provide a new criteria to identify the minimum resolution a simulation must have as a function of signal-to-noise ratio in order for the numerical relativity waveform to be indistinguishable from a true signal. This criteria can be applied to any finite-differencing numerical relativity code with multiple simulations of differing resolutions for the desired binary parameters and waveform length. We apply this criteria to binary systems of interest with the fourth-order `MAYA` code to obtain the first estimate of the minimum resolution a simulation must have to be prepared for next generation detectors.

I. INTRODUCTION

Laser Interferometer Gravitational-wave Observatory (LIGO) and Virgo [1,2] have ushered in the field of gravitational wave (GW) astronomy, a field that will enter a new era as the sensitivity of GW observatories improve and access new GW frequency bands [3,4]. Together with experiment and data analysis, theoretical modeling, analytical and numerical, has been an essential partner in the success of the GW enterprise; therefore, modeling must match the evolution in the increase in sensitivity and reach of current and future detectors.

Modeling of waveforms provided by numerical relativity (NR) has played a crucial role in the detection and interpretation of GWs from merging black holes (BHs) and neutron stars [5–7]. The waveforms extracted from NR simulations form the basis of GW data analysis that have been used to construct models [6,8–12], in direct analysis of the data [13,14], and as injections to stress test the detection pipeline [15].

Of interest to the broad GW community is, therefore, investigating whether current NR codes have the capability to produce waveforms with the accuracy needed to unveil the wealth of information in the data collected by future detectors. While today's NR simulations produce waveforms for which the numerical errors are less significant than the noise associated with the current detectors, this will likely change as the sensitivity of the detectors increase, especially considering the potential for high signal-to-noise ratio (ρ)

detections of binary black holes (BBHs). In order to assess the challenge such high ρ detections pose for NR, this paper provides a new criteria to compute the minimum resolution that a BBH simulation must have as a function of ρ in order for the NR waveform to be indistinguishable from the true signal. We apply this criteria to various systems to obtain the first estimates the minimum resolution simulations must have to be prepared for the high ρ signals expected of future GW detectors.

Differences between a template waveform and a GW signal could have many origins, including, but not limited to, using the "wrong" theory of gravity, using an approximate theory of gravity, or having different parameters between the system and template. Such errors or missing physics in the template waveform have the potential to cause misleading or incorrect results. Assuming general relativity (GR) is the correct gravitational theory, the NR solutions to the vacuum Einstein equations, as well as the waveforms extracted from the solutions, only have errors associated with numerics. This is in contrast with simulations containing neutron stars where the microphysics of the stars are not well understood nor is the impact of possible missing physics on the waveforms [16]. We will focus only on waveforms generated by evolving BBHs in vacuum under Einstein's theory of GR. Figure 1 shows an example of how the use of a low resolution template, one with significant discretization errors, can lead to residuals remaining in the data after the template is used to match the signal. This is demonstrated for an unequal mass binary of
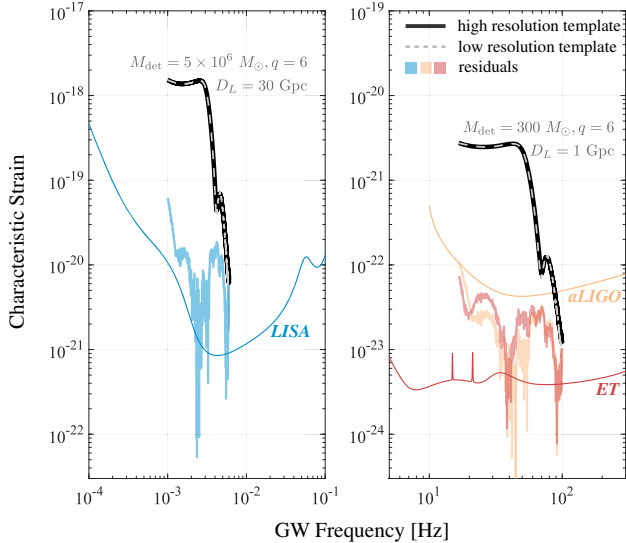
FIG. 1. Strains (gray) for $q = 6$ sources with an aligned spin of $a = 0.2$ on the larger BH; also plotted are noise curves and the residuals remaining in the data after using a low resolution template to match the signal (high resolution waveform).

FIG. 2. Strain (black line) of a high resolution $(q, \iota) = (6, 15^o)$ source with an aligned spin of $a = 0.2$ on the larger BH for LISA at a distance of 30 Gpc, $\rho = 976$. The blue dashed line is a low resolution waveform of the same source parameters, with the solid blue line denoting the residual resulting from using it as the template. The dark red line is a high resolution template containing only the $(l, m) = (2, 2)$ mode, with the faint red line showing the residual resulting from using it as the template waveform.

mass ratio $q = 6$ with a small spin of 20% maximal on the larger BH. In order to consider current detectors as well as future ground and space-based detectors, we show this in comparison to the noise curves of the Laser Interferometer Space Antenna (LISA) [17], Einstein Telescope (ET) [4], and Advanced LIGO at design sensitivity [18,19]. The residual remaining in Cosmic Explorer (CE) [20,21] is comparable to that shown in ET.

The importance of sufficient resolution is also critical when higher-order modes are relevant, such as in unequal mass ratio and inclined binaries. We show in Fig. 2 the strain of the same binary seen in Fig. 1 but now at an inclination of $\iota = 15^0$ for LISA, along with two residuals [3,22]. The blue dashed line is a low resolution waveform and the solid blue line is the residual resulting from using that waveform as the template in matched filtering. The dark red line is a high resolution waveform containing only the $(l, m) = (2, 2)$ mode, with the faint red line showing the residual resulting from using it as the template waveform. Notice that the two residuals are comparable, both in strength and even in structure for this case, although we note that the structure of the residual will change depending on the detector as well as the intrinsic and extrinsic parameters of the BBH.

Several studies have explored the potential impact that numerical errors could have on interpreting LIGO data [15,23–25], including bounds on the numerical errors necessary for detection as well as for measurement [23,26,27]. Reference [24] presents follow up work detailing different methods of assessing the accuracy of waveforms and the appropriate scenarios for each measure. Reference [28] discusses the accuracy requirements for
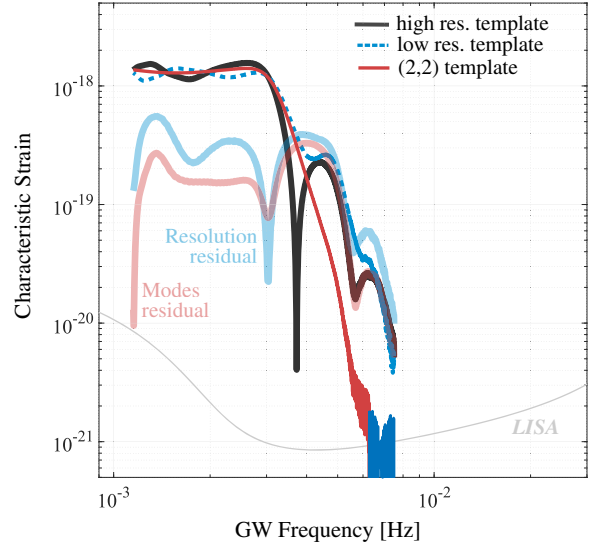
modeled waveforms for third-generation ground-based detectors and the relative errors in the NR waveforms used to build the models.

This paper expands on these works in several ways. Foremost, focusing on the impact of the errors associated with NR simulations of BBHs, we introduce a criteria to assess the errors that arise from the discrete resolution in NR and estimate the minimum resolution required of NR simulations to produce waveforms indistinguishable from the true signal as a function of ρ. We then apply this criteria to several BBH systems in the context of current detectors, third-generation ground detectors such as ET [4,29], and space-based LISA [17]. We also demonstrate how using templates with low resolution may leave residuals behind that could potentially obscure or be confused with higher-order modes.

II. NR WAVEFORMS

Our results are based on the Maya (formerly known as Georgia Tech) catalog of waveforms [30] produced using the MAYA code [31–34], a branch of the Einstein Toolkit [35] which is an NR finite-differencing code that evolves the Baumgarte-Shapiro-Shibata-Nakamura (BSSN) formulation [36,37] built upon Cactus, with mesh refinement from Carpet [38]. The simulations used in this study were performed on a grid with 10 refinement levels with the largest grid radii being 409.6 M and the

smallest grid radii being 0.2 M (0.1 M) for mass ratios of $q = 1$ ($q = 6$). The resolution of the simulation is defined by the spacing of the grid points on the finest mesh. The inspiral parameters quoted for this study are computed at the beginning of the simulation, but there is evidence that the excess radiation emitted at the beginning of an NR simulation does not significantly impact the values of the parameters [39].

As with all BSSN codes, our MAYA code computes waveforms from the Weyl Scalar Ψ_4 extracted at a finite radius away from the BBH and then extrapolated to infinity [40]. For this study, all waveforms have been analyzed at the original extracted radius of 75 M, in order to isolate only the impact of resolution. While extrapolating the waveform to infinite radius makes the waveform more accurate to a true observed signal, by comparing all our waveforms at 75 M, we are considering our "true" signal as it would appear at 75 M. We have repeated this at multiple extraction radii and our results do not change. We therefore do not expect extracting the waveforms to infinite radius to change the impact of resolution, so we leave it at 75 M for simplicity and error orthogonalization.

The strain, h, is given by the second time integral of Ψ_4. To facilitate analysis, the strain is decomposed in terms of spin-weighted spherical harmonics ${}_{-2}Y_{l,m}$, of which the $(l, m) = (2, 2)$ quadrupole mode is generally the most dominant. In the present work, we only use the modes: (2, 1), (2, 2), (3, 2), (3, 3), (4, 3), and (4, 4).

For the binary masses detected and expected, NR simulations are not always able to produce waveforms with enough cycles to cover the sensitive frequency range of the LIGO and Virgo detectors. This will be even more significant for LISA, CE, and ET. To circumvent this, NR waveforms are stitched to approximates (e.g., post-Newtonian), thus creating hybridized waveforms [41]. However, since the goal of this paper is to analyze specifically the truncation error associated with limited NR resolution, we are using only the NR waveform and computing the relevant quantities over the frequency range spanned by it. This analysis does not cover the entire frequency band as to do so with only NR waveforms would be prohibitively expensive in computer time and to add information from other methods (model waveforms or post-Newtonian) would introduce new error sources. For this analysis, we primarily consider total masses in the detector frame of $M_{\text{det}} = 300\ M_\odot$ for terrestrial detectors (CE, ET, and LIGO) and $M_{\text{det}} = 5 \times 10^6\ M_\odot$ for LISA. For the NR waveforms utilized in this study, this means for terrestrial detectors that we use a starting frequency of $f_0 = 6.8$ Hz for the equal mass scenario and $f_0 = 15.9$ Hz for the case with $q = 6$. For LISA we use a starting frequency of $f_0 = 4.1 \times 10^{-4}$ Hz for the equal mass scenario and $f_0 = 9.5 \times 10^{-4}$ Hz for the case with $q = 6$. The equal mass simulation spans the full frequency range of LIGO for the mass of $M_{\text{det}} = 300\ M_\odot$. The other cases do not span the full frequency range due to the limited number of cycles. This can be seen for the $q = 6$ case in Fig. 1. Since NR errors accumulate throughout the simulation, we expect the errors to grow for longer waveforms; therefore, the estimates of necessary resolution provided in the final section of this paper form a lower bound on the errors with respect to the number of cycles.

III. CRITERIA FOR ASSESSING ACCURACY

A waveform h_i extracted from an NR simulation will differ from the exact solution h by an error δh_i; that is, $h_i = h + \delta h_i$. Consider a code that uses finite differencing, to leading order we have $\delta h_i = c\Delta_i^\alpha$. Here α is the convergence rate of the code, c depends on derivatives of h, and Δ_i is the characteristic discretization scale, or grid-spacing, used in the simulation. Due to the use of adaptive mesh refinements, Δ_i will refer to the grid spacing of the finest mesh.

By carrying out simulations of different resolutions, one can determine the convergence rate α of the code and extrapolate h_i to infinite resolution and, in principle, obtain h in a process called Richardson extrapolation [42]. Computing matches between a finite resolution template and the Richardson extrapolated waveform would be an ideal way to quantify the errors associated with limited resolution. However, effects from boundary refinements [38], extrapolations during temporal stepping, and outer boundary conditions, to name a few, make the process of Richardson extrapolation more challenging. While this prevents us from computing the infinite resolution waveform, we can compute the error a finite resolution waveform will have with an infinite resolution waveform, and thus the minimum resolution necessary for indistinguishability. To approximate the absolute truncation errors of a given resolution, we compute the relative errors between multiple simulations of different resolutions and, by doing this for multiple pairs of resolutions, compute our codes convergence rate and express the necessary minimum resolution for indistinguishability as a function of ρ.

Let us consider the overlap of two NR waveforms, h_1 and h_2:

$$\mathcal{O}[h_1, h_2] \equiv \frac{\langle h_1|h_2\rangle}{\sqrt{\langle h_1|h_1\rangle\langle h_2|h_2\rangle}}, \qquad (1)$$

where

$$\langle h_1|h_2\rangle = 2\int_{f_0}^{\infty} \frac{h_1^* h_2 + h_1 h_2^*}{S_n}\, df, \qquad (2)$$

with S_n being the one-sided power spectral density of the detector, and $*$ denoting the complex conjugate. Since h_1 and h_2 both scale with $1/$distance, the distance cancels and the overlap is independent of distance and ρ. Expanding Eq. (1) to second order in the truncation error [32] gives

$$\mathcal{O}[h_1, h_2] \approx 1 - \frac{1}{2}(\Delta_2^{\alpha} - \Delta_1^{\alpha})^2 \frac{\langle c|c \rangle}{\langle h|h \rangle}[1 - \mathcal{O}^2[h, c]]. \quad (3)$$

Noting that c depends on derivatives of h, we can approximate that $\mathcal{O}^2[h, c] \approx 0$ and write Eq. (3) in terms of the mismatch, $\epsilon = 1 - \max_{t_0 \phi_0} \mathcal{O}$, as

$$\epsilon[h_1, h_2] = \frac{\beta^2}{2}(\Delta_2^{\alpha} - \Delta_1^{\alpha})^2, \quad (4)$$

with $\beta^2 = \langle c|c \rangle / \langle h|h \rangle = \langle c|c \rangle / \rho^2$ and $\rho = \langle h|h \rangle^{1/2}$. The mismatch, and therefore β, depends upon the intrinsic source parameters as well as the orientation and sky position of the binary. It is independent of the distance to the source and therefore the overall ρ of the signal. This also implies that, to first order, $\langle c|c \rangle$ is proportional to ρ^2.

Following Ref. [23], an NR waveform will be indistinguishable by the detector from the true signal if and only if $\langle \delta h | \delta h \rangle < 1$, or equivalently $\Delta^{2\alpha} \langle c|c \rangle < 1$. We propose a new version of this criteria for determining accuracy written in terms of β as

$$1/\Delta > (\rho\beta)^{1/\alpha}, \quad (5)$$

providing a *direct* computation between ρ and the minimum necessary resolution, expressed as number of points per length M.

Our definition of β also allows us to estimate the fractional loss of ρ due to numerical errors:

$$\frac{\delta\rho}{\rho} = \frac{\rho_i - \rho}{\rho} = \sqrt{\frac{\langle h_i | h_i \rangle}{\langle h|h \rangle}} - 1 \approx \frac{1}{2}\Delta^{2\alpha}\beta^2. \quad (6)$$

This can be used to estimate the decrease in detection rate due to the discretization error for given binary systems.

The criteria presented in Eqs. (5) and (6) can be applied to any finite-differencing code. The value of α will depend only on the numerical methods, but β will depend upon the parameters of the binary and the length of the waveforms. In the following section, we apply the criteria to our fourth-order finite-differencing code to obtain the first estimate of the resolutions which will be necessary when generating waveforms for analysis with future GW detectors.

IV. APPLYING ACCURACY CRITERIA TO DETECTORS

Once we obtain values for α and β, Eq. (5) provides the minimum resolution necessary for an NR waveform to be indistinguishable from a signal of the same parameters as a function of ρ. Using simulations with multiple different resolutions, we compute mismatches ϵ to obtain β from Eq. (4) for various systems. Unless otherwise specified, we consider masses such that the merger occurs approximately at the most sensitive frequency within the detector,

$M_{\text{det}} = 300\, M_{\odot}$ for terrestrial detectors (CE, ET, and LIGO) and $M_{\text{det}} = 5 \times 10^6\, M_{\odot}$ for LISA. We consider simulations with ~ 7 gravitational wave cycles, and the values of β may change for longer waveforms. Because we have found that the choice of sky location has minimal effect, we choose the sky location such that only the $+$ polarization is observed.

To compute α we make use of a $q = 1$ BBH system observed face-on with an aligned, dimensionless spin of $a = 0.6$ for which we have multiple resolutions. By keeping the higher resolution waveform fixed at $\Delta_1 = M/200$ and varying the lower resolution template, we compute $\alpha = 4$, as can be seen in Fig. 3. As our simulations are performed using sixth-order spatial-finite-differencing and fourth-order Runge-Kutta for time evolution, this value of the convergence rate is consistent. There are other aspects of the simulations, such as the Berger-Oliger evolution scheme, which could cause additional sources of error, possibly with different convergence rates. Future work should be done to explore each of these other potential sources of error.

We explore the values of β for three different BBH systems each for LIGO, CE, ET, and LISA. For the equal mass BBH case, we keep the higher resolution waveform fixed at $\Delta_1 = M/200$ and consider lower resolutions of $\Delta_2 = M/80$, $M/120$, and $M/140$. Using these, we compute $\beta \approx 10^6$ for all three detectors. For unequal mass simulations, finer resolution is required to fully resolve the smaller initial black hole. Therefore, for a $q = 6$ BBH with the more massive BH having an aligned, dimensionless spin of $a = 0.2$, we compare resolutions of $\Delta_1 = M/280$ and $\Delta_2 = M/200$. We obtain $\beta \approx 10^7$ when the binary is observed with $\iota = 0^o$ and $\beta \approx 5 \times 10^8$ when observed
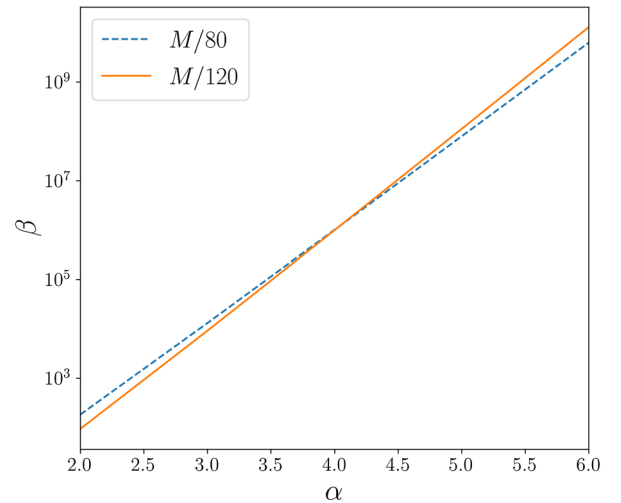

FIG. 3. Plot of β vs α for a $q = 1$ BBH system observed face-on with an aligned, dimensionless spin of $a = 0.6$ obtained using a high resolution of $M/200$ and low resolutions of $M/80$ (dashed blue) and $M/120$ (solid orange). They converge at $\alpha = 4$ and $\beta \approx 10^6$.
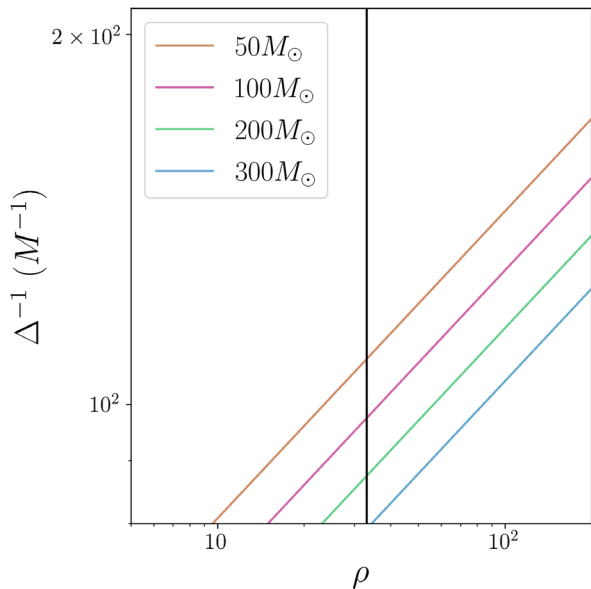
FIG. 4. Plot of Eq. (5) providing the minimum resolution necessary for an NR simulation, expressed as points per length M, for a signal of a given signal-to-noise ratio for a binary with $(q, \iota) = (1, 0^o)$ and an aligned spin of $a = 0.6$ for both BHs as observed with LIGO for several M_{det}. The vertical line shows $\rho = 33$, the highest ρ observed by LIGO through O3a [43,44].

with $\iota = 15^o$, in each of the detectors. While these values of β do change with total mass, they remain at the same order of magnitude.

Figure 4 shows Eq. (5) for a binary system with $(q, \iota) = (1, 0^o)$ and an aligned spin of $a = 0.6$ for both BHs as observed by LIGO for several M_{det}. This provides the minimum resolution necessary for an NR simulation, expressed as points per length M, as a function of ρ. The vertical line shows $\rho = 33$, the highest ρ observed by

LIGO through O3a [43,44]. The BBH case in this figure is characteristic of most of the $q \approx 1$ BBH systems observed so far. Since the NR waveforms used in the data analysis of those signals had resolutions $\Delta < M/120$, they were not distinguishable by LIGO from the true signal.

Looking towards the future detectors as well, Eq. (5) is plotted in Fig. 5 for three detectors: a second-generation detector (LIGO), a third-generation terrestrial detector (ET), and a space-based detector (LISA). The results for CE are extremely comparable to those for ET. Each of the lines shows the minimum resolution necessary for an NR waveform to be indistinguishable from the true signal of the same parameters with a given ρ. This indistinguishability considers only errors due to limited resolution and the frequency range spanned by our NR waveforms. The blue line is for a binary with $(q, \iota) = (1, 0^o)$ and $a = 0.6$ for both BHs. The solid red line is for a binary with $(q, \iota) = (6, 0^o)$ with $a = 0.2$ for the larger BH. The dashed red line is for a binary with $(q, \iota) = (6, 15^o)$ with $a = 0.2$ for the larger BH. The horizontal line shows the highest resolution Maya waveform in the LIGO and Virgo Collaboration (LVC) catalog ($\Delta = M/400$).

Within all four detectors considered, it appears that for low mass ratio cases, current NR waveforms will be sufficient at the expected values of ρ. For the $(q, \iota) = (6, 0^o)$ case, NR waveforms at our current highest resolution ($\Delta = M/400$) would be sufficient for $\rho < 800$ for each of the detectors. Since it is expected that LISA, CE, and ET will be able to detect signals in the hundreds or thousands, it is clear from Fig. 5 that one would require resolutions of at least $\Delta \approx M/600$. The situation gets more challenging if the source has inclination, allowing higher modes to be more observable. For CE, ET, and LISA in the case $(q, \iota) = (6, 15^o)$, resolutions at the level of $\Delta \approx M/10^3$ are needed to accurately reach $\rho \approx 10^3$.
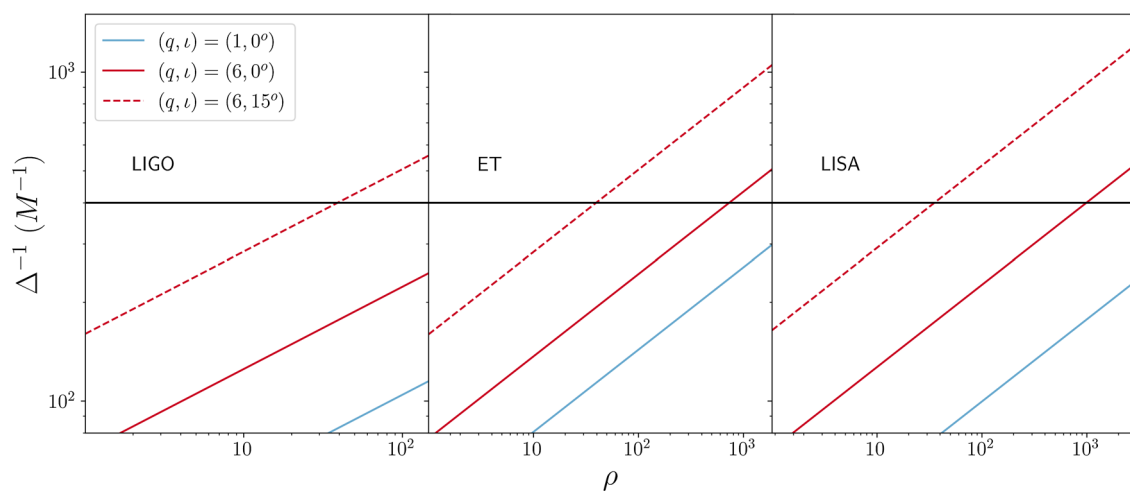

FIG. 5. Plot of Eq. (5) providing the minimum resolution necessary for an NR simulation, expressed as points per length M, for a signal of a given signal-to-noise ratio for various binary sources. The blue line is for a binary with $(q, \iota) = (1, 0^o)$ and $a = 0.6$ for both BHs. The solid red line is for a binary with $(q, \iota) = (6, 0^o)$ with $a = 0.2$ for the larger BH. The dashed red line is for a binary with $(q, \iota) = (6, 15^o)$ with $a = 0.2$ for the larger BH. The horizontal line shows the highest resolution Maya waveform in the LVC catalog ($\Delta = M/400$).

V. CONCLUSIONS

We have provided a new criteria to determine the resolution needed in NR finite-differencing codes to produce waveforms that are indistinguishable by the LIGO, LISA, CE, and ET detectors from the real signal, assuming that the template and the signal have the same parameters. This criteria can be applied to any finite-differencing code provided there exists multiple simulations of differing resolutions for a given binary system.

By applying this criteria to simulations with ~ 7 gravitational wave cycles generated with a fourth-order finite-differencing code, we showed that for detections such as the ones obtained by LIGO so far, with $\rho < 40$, current finite-difference codes are capable of producing adequate waveforms if $\Delta < M/120$. We also showed that for high mass ratio or inclined binaries, where higher modes play an important role, NR codes need to improve significantly. To accurately study signals with values of ρ above a thousand, fourth-order finite-difference NR codes would have to efficiently scale to resolutions of at least $\Delta < M/700$. At those resolutions, to obtain even 7 orbits, we would require approximately 16 nodes on a Stampede equivalent cluster for about 30 days, a very heavy computational load for even the minimum requirements.

Waveforms will need to contain more orbits, particularly for LISA due to its sensitivity and frequency range. Covering the necessary cycles in NR simulations will result in increasing the computation time and the minimum resolution requirements due to accumulated errors. Rather than relying solely on NR, BBH waveforms will likely be hybridized with post-Newtonian and/or used in models, introducing new sources of error to be estimated in future work.

Additionally, in order to accurately analyze simulations with inclination such that higher modes become more prominent, even finer resolutions will be required, increasing the necessary node count and time. The speed decays as a polynomial with $1/\Delta$, and the same simulation at a resolution of $M/1000$ would take more than 60 days. Current finite-differencing codes do not continue to scale efficiently with an increasing number of nodes, so these speeds would not be improved with increased computational resources.

Being able to reach resolutions for template indistinguishability is important because, as we demonstrated, residuals resulting from using lower resolution templates could be comparable to those resulting from ignoring higher modes entirely. This is particularly important since it is expected that LISA and third-generation detectors will observe numerous signals concurrently. Furthermore, the models used in data analysis are trained on NR waveforms; their accuracy is directly limited by that of NR. If we are incapable of providing accurate, indistinguishable NR waveforms, we will not be able to maximize the scientific return from next generation detectors.

While this paper investigates the relationship between resolution and ρ, there are alternative ways to increase the convergence rate of the codes, including increasing the finite-differencing order or implementing more efficient differencing schemes. The need for high quality NR waveforms may be alleviated if the very high ρ signals are not coincident in the detectors, allowing on-demand NR simulations to be deployed per high ρ event.

Our next step is to perform a parameter estimation study to understand how this NR truncation error translates to uncertainty in the physical parameters of the source. Furthermore, the present work was done using the methodology typical for LIGO data analysis, and simply using the noise curves for each detector. However, LISA's data analysis will be notably more complicated, and it will be a crucial future step to study the impact of these errors with LISA's data analysis machinery [45]. Additionally, using the techniques discussed here, we can explore the impact of other errors including but not limited to those caused by extraction radius and boundary conditions.

[1] The LIGO Scientific Collaboration, Classical Quantum Gravity **32,** 074001 (2015).

[2] F. Acernese *et al.* (VIRGO Collaboration), Classical Quantum Gravity **32,** 024001 (2015).

[3] P. A. Seoane *et al.* (eLISA Collaboration), arXiv:1305 .5720.

[4] M. Punturo *et al.*, Classical Quantum Gravity **27,** 194002 (2010).

[5] B. Abbott *et al.* (LIGO Scientific and Virgo Collaborations), Phys. Rev. Lett. **119**, 161101 (2017).

[6] B. Abbott *et al.* (LIGO Scientific and Virgo Collaborations), Astrophys. J. Lett. **892**, L3 (2020).

[7] M. Shibata, S. Fujibayashi, K. Hotokezaka, K. Kiuchi, K. Kyotoku, Y. Sekiguchi, and M. Tanaka, Phys. Rev. D **96**, 123012 (2017).

[8] M. Hannam, P. Schmidt, A. Bohé, L. Haegel, S. Husa, F. Ohme, G. Pratten, and M. Pürrer, Phys. Rev. Lett. **113**, 151101 (2014).

[9] A. Bohé *et al.*, Phys. Rev. D **95**, 044028 (2017).

[10] S. Khan, S. Husa, M. Hannam, F. Ohme, M. Pürrer, X. Jiménez Forteza, and A. Bohé, Phys. Rev. D **93**, 044007 (2016).

[11] J. Blackman, S. E. Field, M. A. Scheel, C. R. Galley, C. D. Ott, M. Boyle, L. E. Kidder, H. P. Pfeiffer, and B. Szilágyi, Phys. Rev. D **96**, 024058 (2017).

[12] S. Husa, S. Khan, M. Hannam, M. Pürrer, F. Ohme, X. Jiménez Forteza, and A. Bohé, Phys. Rev. D **93**, 044006 (2016).

[13] B. P. Abbott *et al.* (LIGO Scientific and Virgo Collaborations), Phys. Rev. D **93**, 122004 (2016); **94**, 069903(E) (2016).

[14] J. Lange *et al.*, Phys. Rev. D **96**, 104041 (2017).

[15] P. Schmidt, I. W. Harry, and H. P. Pfeiffer, arXiv:1703 .01076.

[16] V. Nedora, S. Bernuzzi, D. Radice, B. Daszuta, A. Endrizzi, A. Perego, A. Prakash, M. Safarzadeh, F. Schianchi, and D. Logoteta, Astrophys. J. **906**, 98 (2021).

[17] T. Robson, N. J. Cornish, and C. Liu, Classical Quantum Gravity **36**, 105011 (2019).

[18] B. P. Abbott *et al.* (KAGRA, LIGO Scientific, and VIRGO Collaborations), Living Rev. Relativity **21**, 3 (2018).

[19] LIGO Scientific Collaboration, LIGO Algorithm Library— LALSuite, free software (GPL) (2018).

[20] D. Reitze *et al.*, Bull. Am. Astron. Soc. **51**, 035 (2019).

[21] S. Dwyer, D. Sigg, S. W. Ballmer, L. Barsotti, N. Mavalvala, and M. Evans, Phys. Rev. D **91**, 082001 (2015).

[22] P. Amaro-Seoane *et al.*, arXiv:1702.00786.

[23] L. Lindblom, B. J. Owen, and D. A. Brown, Phys. Rev. D **78**, 124020 (2008).

[24] L. Lindblom, Phys. Rev. D **80**, 064019 (2009).

[25] I. Hinder *et al.*, Classical Quantum Gravity **31**, 025012 (2014).

[26] E. E. Flanagan and S. A. Hughes, Phys. Rev. D **57**, 4566 (1998).

[27] M. Miller, Phys. Rev. D **71**, 104016 (2005).

[28] M. Pürrer and C.-J. Haster, Phys. Rev. Research **2**, 023151 (2020).

[29] M. Abernathy *et al.*, Einstein gravitational wave Telescope conceptual design study, EGO (2011).

[30] K. Jani, J. Healy, J. A. Clark, L. London, P. Laguna, and D. Shoemaker, Classical Quantum Gravity **33**, 204001 (2016).

[31] F. Herrmann, I. Hinder, D. Shoemaker, and P. Laguna, Classical Quantum Gravity **24**, S33 (2007).

[32] B. Vaishnav, I. Hinder, F. Herrmann, and D. Shoemaker, Phys. Rev. D **76**, 084020 (2007).

[33] J. Healy, J. Levin, and D. Shoemaker, Phys. Rev. Lett. **103**, 131101 (2009).

[34] L. Pekowsky, R. O'Shaughnessy, J. Healy, and D. Shoemaker, Phys. Rev. D **88**, 024040 (2013).

[35] F. Loffler *et al.*, Classical Quantum Gravity **29**, 115001 (2012).

[36] T. W. Baumgarte and S. L. Shapiro, Phys. Rev. D **59**, 024007 (1998).

[37] M. Shibata and T. Nakamura, Phys. Rev. D **52**, 5428 (1995).

[38] E. Schnetter, S. H. Hawley, and I. Hawke, Classical Quantum Gravity **21**, 1465 (2004).

[39] K. Higginbotham, B. Khamesra, J. P. McInerney, K. Jani, D. M. Shoemaker, and P. Laguna, Phys. Rev. D **100**, 081501 (2019).

[40] H. Nakano, J. Healy, C. O. Lousto, and Y. Zlochower, Phys. Rev. D **91**, 104022 (2015).

[41] P. Ajith *et al.*, Classical Quantum Gravity **29**, 124001 (2012); **30**, 199401(E) (2013).

[42] L. F. Richardson and R. T. Glazebrook, Proc. R. Soc. Ser. A **83**, 335 (1910).

[43] B. P. Abbott *et al.* (LIGO Scientific and Virgo Collaborations), Phys. Rev. X **9**, 031040 (2019).

[44] R. Abbott *et al.* (LIGO Scientific and Virgo Collaborations), Phys. Rev. X **11**, 021053 (2021).

[45] K. A. Arnaud *et al.*, AIP Conf. Proc. **873**, 619 (2006).

Correction: A minor typographical error in Eq. (5) has been fixed.